Second-Order Analytic Extension of Eigenvalues for Fast Frequency Sweep Analysis of RF Circuits

Hongliang Li, *Graduate Student Member, IEEE*, Jian-Ming Jin, *Fellow, IEEE*, Douglas R. Jachowski, *Member, IEEE*, and Robert B. Hammond, *Life Member, IEEE*

Abstract—A second-order analytic extension of eigenvalue (AEE) method is presented and investigated for efficiently computing the Z-parameters of passive RF circuits over a wide frequency band with full-wave accuracy. The Z-parameters of an RF circuit are first extracted based on a full-wave simulation on sampling frequencies and then decomposed into eigenmodes, whose eigenvalues are analytically extended to all other frequencies within the frequency band of interest based on functional equations constructed from second-order series and parallel RLC circuits. An eigenvector-eigenvalue identity is adopted to compute the frequency-dependent eigenvectors from the eigenvalues of the submatrices, which are used in the expansion of the Z-parameters. A comparison with full-wave solutions is given for the second-order AEE where four frequencies are employed to accurately approximate the Z-parameters and predict the frequency response over the entire band of interest that goes to much higher frequencies than the first-order AEE. With this, the previously developed first-order AEE for a quasi-static analysis is successfully extended to much higher frequencies. Numerical examples are provided to validate the accuracy and demonstrate the capability of the second-order AEE. It is found that the second-order AEE is very accurate for modeling RF circuits with electrical sizes up to one wavelength that possibly contains resonances, as compared to the first-order AEE, which is applicable only to RF circuits with electrical sizes smaller than one-tenth to one-fifth of a wavelength that contains no resonance.

Index Terms—Eigenmode analysis, fast frequency sweep, RF device modeling.

I. INTRODUCTION

FAST frequency sweep analysis of RF circuits is critical for the design and optimization of novel circuits and devices in electronic gadgets and wireless communications. Over the past three decades, a variety of fast frequency sweeping techniques have been developed to predict the characteristics of RF circuits over a broad frequency band of interest based on simulations at a few sampling frequencies. These techniques are either based on physical models such as lumped equivalent circuits [1]–[6] or mathematical models such as those employed in the model-based parameter extraction (MBPE) [7], [8], the asymptotic waveform evaluation (AWE) [9]–[11], the Padé via Lanczos (PVL) [12]–[15], and the solution space projection (SSP) [16]–[18]. Mathematically based techniques are found to be more general and powerful as they do not require a physical model that has to accurately mimic the true characteristics of the original circuits and they are applicable to any circuit configuration and any frequency range.

Recently, we developed a new method based on an analytic extension of eigenvalues (AEEs) for the quasi-static analysis of miniature RF circuits [19]. In this method, a standard eigenvalue problem based on the extracted impedance parameters is solved at one or two sampling frequencies, and the computed eigenvalues are analytically extended to all other frequencies in the frequency band of interest based on a functional equation formulated from RLC circuits. The Z-parameters over the entire frequency band can then be computed very quickly from their eigenexpansion in terms of the eigenvectors. In [19], we tested this method on miniature RF circuits, where a simple series RLC circuit is used to extend the eigenvalues and the eigenvectors are assumed constant within the entire frequency band. We found this quasi-static AEE to be very accurate and efficient for a circuit or component whose electrical size is smaller than one-tenth to one-fifth of a wavelength. However, significant discrepancies are observed at higher frequencies since the simple series RLC circuit is unable to capture the variations of the eigenvalues, and the assumption that the eigenvectors are frequency-independent is no longer valid. Although for some RF circuits one can divide them into subcomponents that satisfy the quasi-static criteria, this approach is not applicable to general RF circuits when such a decomposition is not feasible. In this article, the quasi-static restriction is alleviated by extending the previously developed AEE to a much higher frequency range so that it can be used for a broader range of applications. For this, the resonant and antiresonant behaviors that occur in the eigenmodes are discussed first, and second-order models are constructed by including more RLC blocks. The frequency-dependent eigenvectors are modeled by a so-called "eigenvector-eigenvalue identity" [20]. Finally, the Z-parameters of the RF circuits are approximated from the full-wave solutions at four frequencies for the case of the second-order AEE, and the frequency response can then be
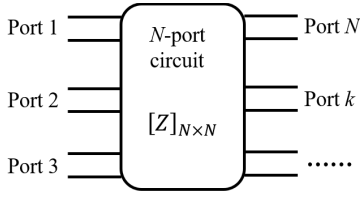
Hongliang Li and Jian-Ming Jin are with the Center for Computational Electromagnetics, Department of Electrical and Computer Engineering, University of Illinois at Urbana–Champaign, Urbana, IL 61801 USA (e-mail: hl23@illinois.edu; j-jin1@illinois.edu).

Douglas R. Jachowski and Robert B. Hammond are with Resonant Inc., Goleta, CA 93117 USA (e-mail: djachowski@resonant.com; bhammond@resonant.com).
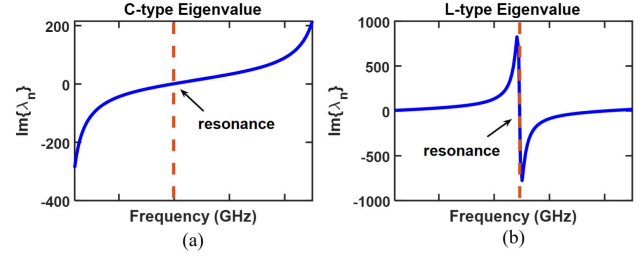
Fig. 1. *N*-port circuit network and *Z*-matrix description.

Fig. 2. C-type and L-type eigenvalues. (a) Frequency behavior of C-type eigenvalues. (b) Frequency behavior of L-type eigenvalues.

predicted quickly with full-wave accuracy. This approach is found to be very accurate and efficient for modeling RF microstrip-type circuits with electrical sizes up to one wavelength that can even possibly contain resonances.

This article is organized as follows. Section II provides a detailed formulation of the AEE on extracted *Z*-parameters; Section III presents several numerical examples to validate the proposed approach and demonstrate the ability to solve practical problems. Finally, this article is concluded in Section IV.

II. FORMULATION

In this section, we first review the basic AEE formulation and discuss the second-order representation of eigenvalues to capture frequency dependence over a broader frequency range. We then present the method to calculate the frequency-dependent eigenvectors which were assumed to be frequency-invariant in the quasi-static analysis.

A. Eigenanalysis on Z-Parameters

The proposed AEE is applied directly to the extracted *Z*-parameters which can be obtained from any full-wave analysis method. Given an *N*-port circuit as shown in Fig. 1, the *Z*-parameters are defined as

$$[Z]\{I\} = \{V\} \tag{1}$$

where $[Z] = [R] + j[X]$ is the *N*-port impedance matrix, $\{I\}$ is the current vector flowing into the ports, and $\{V\}$ is the voltage vector on the ports. Now consider a standard eigenvalue problem

$$[Z]\{v_n\} = \lambda_n\{v_n\} \tag{2}$$

where λ_n are the eigenvalues and $\{v_n\}$ are the corresponding eigenvectors which are referred to as characteristic currents or eigencurrents. Since $[Z]$ is not Hermitian, λ_n and $\{v_n\}$ are complex. However, for reciprocal circuits whose impedance matrix is complex symmetric, the eigenvectors are orthogonal in a transpose sense

$$\{v_m\}^{\mathrm{T}}\{v_n\} = \xi_n\delta_{mn} \tag{3}$$

where δ_{mn} denotes the Kronecker delta function, the superscript $\{\cdot\}^{\mathrm{T}}$ represents the transpose, and $\xi_n = \{v_n\}^{\mathrm{T}}\{v_n\}$. The orthogonal eigenvectors $\{v_n\}$ can be chosen as a set of modes to expand any current vector $\{I\}$ flowing into the ports

$$\{I\} = \sum_n \alpha_n\{v_n\}. \tag{4}$$

The expansion coefficients α_n are to be determined depending on whether the network is excited by a current or voltage

source. For a voltage excitation $\{V_{\mathrm{src}}\}$, substituting (4) into (1) and testing it with $\{v_m\}$ yields

$$\sum_n \alpha_n\{v_m\}^{\mathrm{T}}[Z]\{v_n\} = \{v_m\}^{\mathrm{T}}\{V_{\mathrm{src}}\}. \tag{5}$$

Because of the orthogonality relationship (3), (5) reduces to

$$\alpha_n = \frac{\{v_n\}^{\mathrm{T}}\{V_{\mathrm{src}}\}}{\lambda_n\xi_n}. \tag{6}$$

For a current excitation $\{I_{\mathrm{src}}\}$, the derivation of the coefficients α_n is very straightforward, and one only needs to take the inner product of (4) with $\{v_m\}$, which gives

$$\alpha_n = \{v_n\}^{\mathrm{T}}\{I_{\mathrm{src}}\}/\xi_n. \tag{7}$$

B. Analytical Extension of Eigenvalues

Next, we examine the physical meaning of the eigenvalues and find an appropriate representation for them. Since the standard eigenvalue decomposition diagonalizes the impedance parameters into

$$[Z] = [v]\begin{bmatrix} \lambda_1 & & & \\ & \lambda_2 & & \\ & & \ddots & \\ & & & \lambda_N \end{bmatrix}[v]^{-1} \tag{8}$$

the eigenvalue λ_n corresponds to the impedance for the *n*th eigenmode.

Through numerical studies, it is found that all the eigenvalues have frequency behaviors that can be categorized into two types: the C- and L-type. For C-type eigenvalues (λ_n^C) as shown in Fig. 2(a), the modal impedance is capacitively dominant at low frequencies and the corresponding eigenvalue has a negative imaginary part. As frequency increases, resonance occurs and the imaginary part of the eigenvalue crosses zero. The behavior of the C-type eigenvalues at low frequencies can be well represented by a series LC circuit model. As for L-type eigenvalues (λ_n^L) as shown in Fig. 2(b), the modal impedance is inductively dominant in a low band below the resonance frequency, and its imaginary part is positive. Around the resonant frequency, the imaginary part reaches a peak value and rapidly changes sign to a negative value. At low frequencies, these eigenvalues exhibit behavior that can be modeled by a parallel LC circuit.

To model various losses evident in device characteristics, a lumped resistance is included in the models based on the
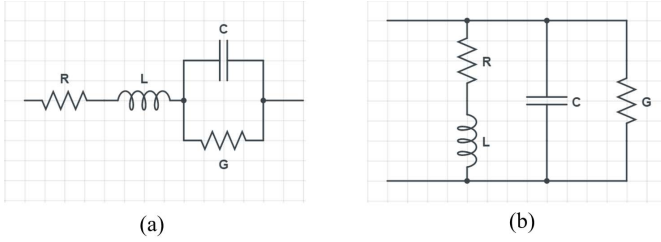
Fig. 3. RLC representations of eigenvalues. (a) Series RLC model for C-type eigenvalues. (b) Parallel RLC model for L-type eigenvalues.

Fig. 4.   Second-order RLC representations for eigenvalues. (a) Second-order parallel RLC model. (b) Second-order series RLC model.

physical loss mechanism. For conductor loss caused by a finite conductivity, a resistor can be added by connecting it in series with the inductor, whereas for dielectric loss, a resistor can be inserted in parallel with the capacitor. The resulting series and parallel circuit models that describe the C- and L-type eigenvalues are shown in Fig. 3(a) and (b). The eigenvalue for each mode can therefore be approximated by either the impedance of the series circuit model (Z_n^s) as

$$\lambda_n^C = Z_n^s = R_n + j\omega L_n + \frac{1}{G_n + j\omega C_n} \tag{9}$$

or the admittance of the parallel circuit model (Y_n^p) as

$$\left(\lambda_n^L\right)^{-1} = Y_n^p = G_n + j\omega C_n + \frac{1}{R_n + j\omega L_n}. \tag{10}$$

In the quasi-static analysis where the overall electrical size of a circuit or component is a small fraction of the wavelength, the eigenvalues are either capacitively or inductively dominant, and there are no zero-crossings and therefore no resonances. A single series circuit model can be used to fit the C-type eigenvalues and a single parallel circuit model can model the L-type eigenvalues, which can be automatically determined by the sign of the imaginary part of the eigenvalues. A full-wave simulation can be performed at two frequencies to extract the characteristic inductance L_n and capacitance C_n, whose values are assumed constant over the frequency range of interest. The modal resistance R_n and conductance G_n, however, are not necessarily to be constant and their behaviors as a function of frequency are supposed to be *a priori* knowledge. Specifically, the frequency-dependent resistance is assumed to vary exponentially as $R_n \sim f^\beta$. For the conductor loss where the skin effect is considered, we have

$$R_n^{\text{cond}} = R_{n0}^{\text{cond}} f^{0.5}. \tag{11}$$

The loss introduced by the absorbing boundary condition (ABC) can be assumed constant, and the conductance corresponding to the dielectric loss varies with frequency as

$$G_n^{\text{diel}} = G_{n0}^{\text{diel}} f. \tag{12}$$

As frequency goes higher, the eigenvalues will cross zero and resonance occurs. One RLC circuit is no longer able to capture the variations since the contribution of higher modes with resonances is no longer negligible. By including more RLC blocks, and specifically, connecting series RLC circuits in parallel or parallel RLC circuits in series, higher order
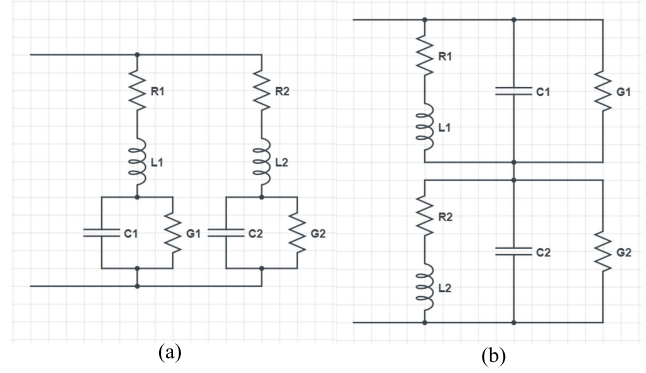
models are obtained as illustrated in Fig. 4. For the Nth-order series RLC model, the eigenvalues are expressed as

$$\frac{1}{\lambda_n^{C,N}} = Y_{\text{tot}}^s = \sum_{i=1}^{N} Y_{ni}^s \tag{13}$$

with

$$Y_{ni}^s = \left(R_{ni} + j\omega L_{ni} + \frac{1}{G_{ni} + j\omega C_{ni}}\right)^{-1} \tag{14}$$

whereas the eigenvalues for the Nth-order parallel RLC model can be written as

$$\lambda_n^{L,N} = Z_{\text{tot}}^p = \sum_{i=1}^{N} Z_{ni}^p \tag{15}$$

with

$$Z_{ni}^p = \left(G_{ni} + j\omega C_{ni} + \frac{1}{R_{ni} + j\omega L_{ni}}\right)^{-1}. \tag{16}$$

In this article, the second-order models consisting of two RLC blocks are used, where the Z-parameters at four frequency points computed by a full-wave analysis are employed to determine R_n, G_n, L_n, and C_n through point-matching. The second order is chosen because 1) a very significant gain in both accuracy and efficiency can be achieved by going from the first to the second order and 2) second-order RLC blocks are still basic enough to model any small distributive circuits. Although in principle, one can increase the order further higher by adding more RLC blocks to improve the accuracy and extend the range of validity to even higher frequencies, it is not practical for engineering applications because 1) the subsequent gains by going beyond the second-order become less significant and 2) the associated computational cost, mostly due to the full-wave simulation at an increased number of sampling frequencies, will increase accordingly. To maintain high efficiency, high orders should be applied to larger circuits or higher frequencies. However, for larger circuits or higher frequencies, standard RLC blocks may not be most suited to model their complicated responses, thus compromising the generality of the method. Based on these considerations, the second-order model is found both sufficient and robust for practical RF circuit design purposes.

To extract R_n, G_n, L_n, and C_n through point-matching, a direct solution of the nonlinear equations in (13) and (15) is tedious, and thus approximations have to be made to simplify the extraction of the parameters. By assuming that the losses are relatively small such that $R_{ni} \ll \omega L_{ni}$ and $G_{ni} \ll \omega C_{ni}$, which hold for most practical applications, the expression in (14) can be approximated as

$$\text{Im}\{Y_{ni}^{\text{s}}\} \approx \frac{\omega C_{ni}}{1 - \omega^2 L_{ni} C_{ni}} \tag{17a}$$

$$\text{Re}\{Y_{ni}^{\text{s}}\} \approx \frac{G_{ni} + \omega^2 C_{ni}^2 R_{ni}}{\left(1 - \omega^2 L_{ni} C_{ni}\right)^2} \tag{17b}$$

and (16) can be approximated as

$$\text{Im}\{Z_{ni}^{\text{p}}\} \approx \frac{\omega L_{ni}}{1 - \omega^2 L_{ni} C_{ni}} \tag{18a}$$

$$\text{Re}\{Z_{ni}^{\text{p}}\} \approx \frac{R_{ni} + \omega^2 L_{ni}^2 G_{ni}}{\left(1 - \omega^2 L_{ni} C_{ni}\right)^2}. \tag{18b}$$

Note that the imaginary parts (17a) and (18a) are exactly the same as the expressions for the corresponding lossless models. These equations are first utilized to extract L_{ni} and C_{ni} from the eigenvalues at four frequencies, which is readily solvable by a nonlinear numerical solver in MATLAB. The values are then substituted into the real parts (17b) and (18b), and the constant parameters in R_{ni} and G_{ni} can be obtained by solving the corresponding linear equations. This process can be iterated a few times until results converge, and convergence is found to occur very quickly.

C. Reconstruction of Eigenvectors and Impedance Parameters

Although the eigenvectors may be assumed to be constant at low frequencies similar to the modal fields of quasi-TEM modes, they vary dramatically with frequency at higher frequencies, especially when discontinuities exist in the structure so that higher order modes are excited. To capture the frequency-dependent behavior of the eigenvectors, a so-called "eigenvector-eigenvalue identity" [20] is utilized. Given a $n \times n$ Hermitian matrix $[A]$ with eigenvalues $\lambda_1(A), \ldots, \lambda_n(A)$, the magnitude of the jth component of the normalized eigenvector v_i for the jth mode is given by

$$|v_{i,j}|^2 = \frac{\prod\limits_{k=1}^{n-1} \left[\lambda_i(A) - \lambda_k(M_j)\right]}{\prod\limits_{k=1, k \neq i}^{n} \left[\lambda_i(A) - \lambda_k(A)\right]} \tag{19}$$

where $\lambda(M_j)$ is the eigenvalue of the submatrix $[M_j]$ obtained by removing the jth row and column of matrix $[A]$. Note that the submatrix $[M_j]$ is actually the impedance matrix with the jth port open; hence the AEE can be applied to $[M_j]$ to obtain the eigenvalues.

The identity (19) yields only information about the magnitude of the components of a given eigenvector but it does not provide the phase of these components. In addition, the Z-parameters are usually not Hermitian for a circuit with loss. Consequently, this identity cannot be applied directly

to our problem. Since the losses in most well-designed RF circuits are very small, the real parts of the eigenvectors dominate over the imaginary parts and contribute more to the characteristic current distribution. Therefore, the eigenvectors can be approximated as real when used in the eigenexpansion of the Z-parameters. Under this assumption, we found that (19) is still applicable when the real part of the right-hand side is taken. Furthermore, if the electrical size of the circuit does not exceed one wavelength, the eigenvectors do not change their polarities, and the sign of each component $v_{i,j}$ can be determined from any sampling frequency. For a circuit whose electrical size is larger than one wavelength, we can decompose it into several smaller subcomponents, perform AEE to each subcomponent, and re-combine them to obtain the characteristics of the entire circuit.

Once the eigenvalues and eigenvectors are approximated from a few sampling frequencies, the impedance parameters can be reconstructed and thus the characteristics of a circuit can be predicted. By definition, Z_{ij} can be founded by driving port j with the current $I_j = 1$, leaving all other ports open-circuited, and measuring the voltage at port i, so that

$$Z_{ij} = \left.\frac{V_i}{I_j}\right|_{I_k=0 \text{ for } k \neq j} = V_i|_{I_j=1, \ I_k=0 \text{ for } k \neq j}. \tag{20}$$

Therefore, we can excite port j and leave all other ports open-circuited, which gives $\{I_{\text{src}}^{(j)}\} = [0 \ldots 0, 1, 0, \ldots, 0]^{\text{T}}$ with only the jth element to be one and all others to be zero. By substituting the current source vector $\{I_{\text{src}}^{(j)}\}$ into the modal expansion in (4), the voltages on the ports can be computed as

$$\{V^{(j)}\} = [Z]\{I_{\text{src}}^{(j)}\} = \sum_n \alpha_n^{(j)}[Z]\{v_n\} = \sum_n \alpha_n^{(j)}\lambda_n\{v_n\} \tag{21}$$

where the coefficients $\alpha_n^{(j)}$ are obtained from (7) as $\alpha_n^{(j)} = \{v_n\}_j^{\text{T}}/\xi_n$. The Z-parameters can finally be written in a compact form as

$$[Z] = \sum_n \lambda_n \{v_n\}\{v_n\}^{\text{T}}/\xi_n. \tag{22}$$

III. NUMERICAL RESULTS

In this section, we present several numerical examples to demonstrate the capability of the proposed AEE approach by comparing the results with the full-wave solution. The finite-element method (FEM) is employed to produce all full-wave results including those at sampled frequencies.

A. Microstrip Line

A microstrip line example is first used to examine the capability of various models to represent the eigenvalues. The test example consists of a conducting strip, which is 0.04 mm wide and 1.0 mm long, and is printed on a substrate with a thickness of 0.15 mm and a dielectric constant of 56, as shown in Fig. 5. The conductor is made of copper with a thickness of 0.01 mm and a conductivity of 5.8×10^7 S/m. The substrate is chosen to be lossy with a dielectric loss tangent of 0.02. The simulation domain that encloses the
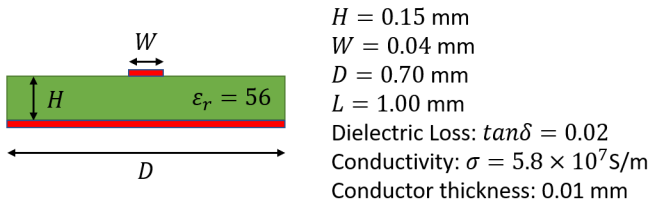
Fig. 5. Numerical example 1: a microstrip line.

$H = 0.15$ mm
$W = 0.04$ mm
$D = 0.70$ mm
$L = 1.00$ mm
Dielectric Loss: $\tan\delta = 0.02$
Conductivity: $\sigma = 5.8 \times 10^7$ S/m
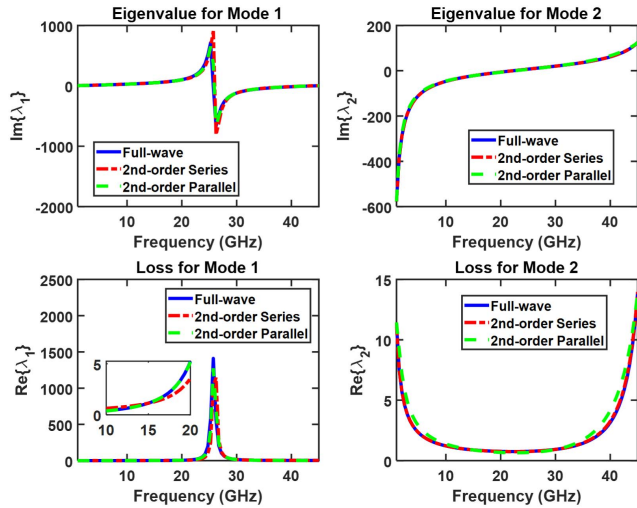Conductor thickness: 0.01 mm

Fig. 6. Eigenvalues of the two modes in example 1 from 1 to 50 GHz using the second-order AEE (with four frequencies at 1, 15, 30, and 45 GHz). Top: imaginary parts. Bottom: real parts.
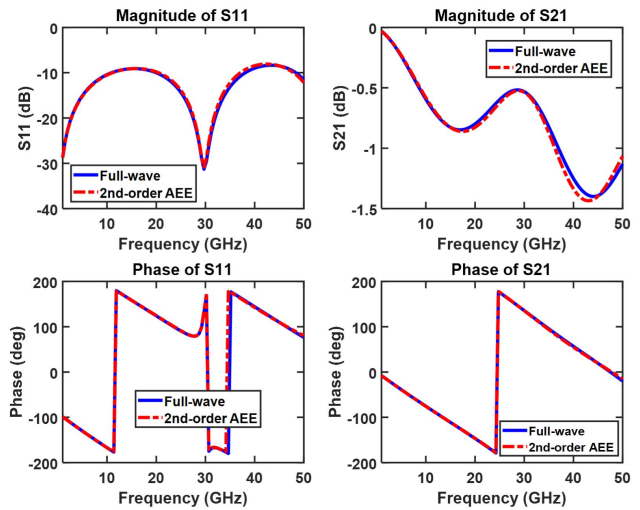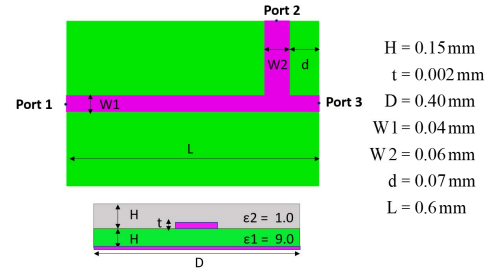

Fig. 7. *S*-parameters for the microstrip line of example 1 from 1 to 50 GHz using the second-order AEE (with four frequencies at 1, 15, 30, and 45 GHz). Top: magnitude. Bottom: phase.

$H = 0.15$ mm
$t = 0.002$ mm
$D = 0.40$ mm
$W1 = 0.04$ mm
$W2 = 0.06$ mm
$d = 0.07$ mm
$L = 0.6$ mm

$\varepsilon 2 = 1.0$
$\varepsilon 1 = 9.0$

Fig. 8. Numerical example 2: three-port microstrip lines.

entire structure is truncated with an ABC that has dimensions of 1.40 mm × 1.10 mm × 1.00 mm.

We first applied the first-order AEE with two frequency points at 0.1 and 15.0 GHz using the parallel *RLC* circuit to fit the inductively dominant mode and a series *RLC* circuit to fit the capacitively dominant mode. The conductor loss with a frequency behavior of $R = R_0 \, f^{0.5}$ and the dielectric loss that varies as $G = G_0 \, f$ are included to model losses in the parameter extraction, which achieved a very good accuracy for the real parts of the eigenvalues. Compared with the solution of full-wave analysis performed directly at each frequency point, an excellent agreement was achieved with the first-order AEE up to 17 GHz. However, at higher frequencies, the first-order models become less and less accurate. In such cases, second-order models can be used to provide more accurate predictions. Here, applying the second-order AEE, we consider a frequency range up to 50 GHz and we choose four sampling frequencies at 1, 15, 30, and 45 GHz. The eigenvalues and the calculated *S*-parameters are presented in Figs. 6 and 7. A comparison between the series and parallel models is also plotted. Unlike the first-order models, the difference between the two second-order models in the capability of fitting the eigenvalues is much smaller. However, it is still recommended to choose proper models for each mode based on the polarity of its eigenvalue such that the series *RLC* circuit is used for C-type modes and

the parallel *RLC* circuit for L-type modes. In this example, mainly the quasi-TEM mode exists, resulting in relatively constant eigenvectors whose values for the two modes are $v_1 = [1, -1]^{\mathrm{T}}/\sqrt{2}$ and $v_2 = [1, 1]^{\mathrm{T}}/\sqrt{2}$, respectively. As can be seen, the second-order AEE provides excellent results all the way up to 50 GHz.

B. Multiport Circuit Analysis

Next, we examine the proposed AEE for the analysis of multiport networks. For this, a three-port circuit is designed, which consists of two connected microstrip lines that are perpendicular to each other, as depicted in Fig. 8. The horizontal line has a width of 0.04 mm and the vertical line is 0.06 mm wide. The entire structure is 0.6 mm long and 0.4 mm wide. Port 1 is excited by a 1.0-A current source, and ports 2 and 3 are both loaded with a 50-Ω resistor. The perfect electrically conducting (PEC) boundary condition is applied to all boundaries except for those where the ports are defined.

Fig. 9 gives the eigenvalues as well as the eigenvectors for all three modes. For a better view, the imaginary parts of the eigenvalues for capacitively dominant modes are inverted. It is clear from the figures that resonances occur, and the eigenvalues change their signs across the resonant frequencies. The AEE utilizes four frequency points equally placed between 0.5 and 90 GHz, and the results are compared with
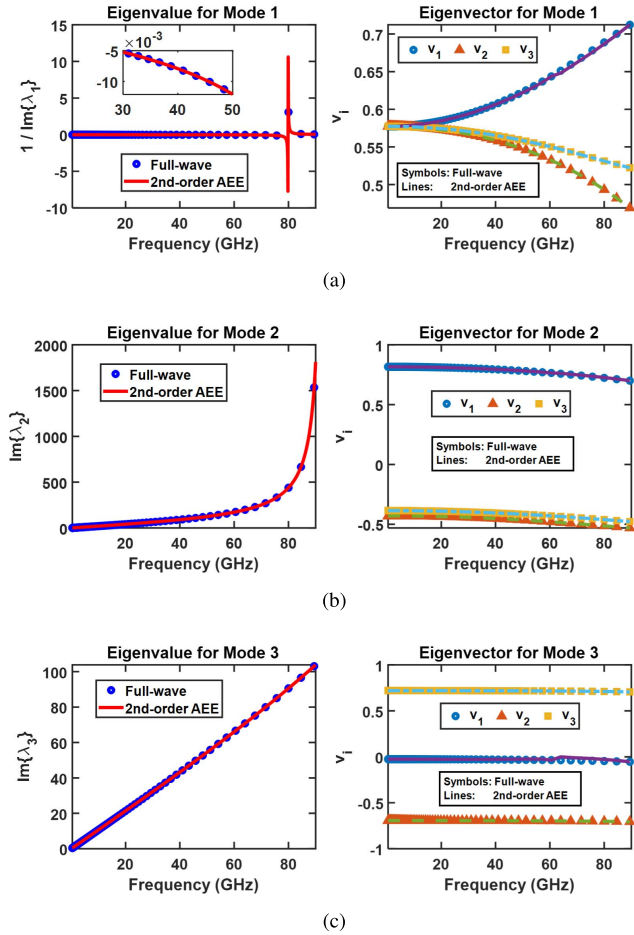
Fig. 9. Eigenvalues and eigenvectors of the three modes in example 2 using the second-order AEE. (a) Mode 1. (b) Mode 2. (c) Mode 3. Left: imaginary parts of the eigenvalues. Right: three components of the eigenvector for each mode.

Fig. 10. Second-order AEE results versus full-wave analysis for example 2. (a) Voltage at port 1. (b) Voltage at port 2. (c) Voltage at port 3.

the full-wave solution. Unlike example 1, the eigenvectors are no longer constant—due to the higher frequencies and higher-order modes excited at the discontinuities. To capture the variation of the eigenvectors with respect to frequency, the "eigenvector-eigenvalue identity" is employed. When the electrical size of the device is smaller than one wavelength, the sign of the eigenvectors may be assumed unchanged and can then be obtained from any sampling frequency. In identity (19), the eigenvalues of all submatrices are required. As mentioned earlier, M_j can be considered to be the Z-parameters with the jth port open, and therefore can also be modeled by the second-order RLC.

The voltages from the AEE and full-wave results at the three ports are compared in Fig. 10(a)–(c). Excellent agreement is observed up to 50 GHz where the relative error is smaller than 0.5%. At higher frequencies, the error increases and the maximum error is around 4% except for some points where the absolute values are small or cross zero. As a comparison, the AEE results without taking into account the frequency variations of the eigenvectors are also presented in Fig. 11 where the eigenvectors are assumed constant by taking the values at the first frequency point. The maximum relative error in this case is 5% below 20 GHz. The accuracy of
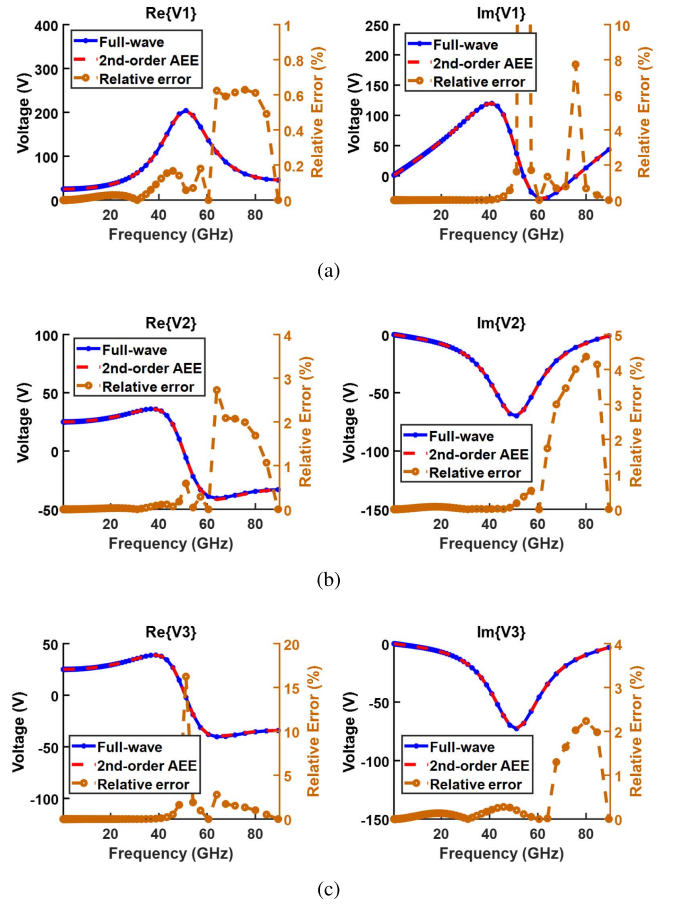
the results indicates that the second-order RLC can correctly represent the eigenvalues, and the "eigenvector-eigenvalue identity" in (19) is able to capture the frequency variation of the eigenvectors. Therefore, the AEE can successfully predict the characteristics of multiport RF circuits that possibly contain resonances. It is also found that the second-order AEE with four frequency points can achieve very high accuracy up to a frequency where the electrical size is about one wavelength.

C. Numerical Modeling of a Low-Pass Filter

To illustrate the practical application of the proposed AEE, a stepped-impedance low-pass filter [21] is analyzed whose dimensions are given in Fig. 12. The filter consists of eight series stubs and is fabricated with microstrip lines with three different characteristic impedances, 50, 20, and 120 Ω. It has a maximally flat response and a cutoff frequency at 2.5 GHz, and the insertion loss at 4 GHz is below −20 dB.

Since the electrical size of the whole device is larger than one wavelength within the frequency range of interest, a direct application of the second-order AEE may not yield an accurate solution over the band. To overcome this problem, we divide the whole structure into four smaller segments with a length of roughly 11 mm, apply AEE to each part, and then cascade the parameters to obtain the characteristics of
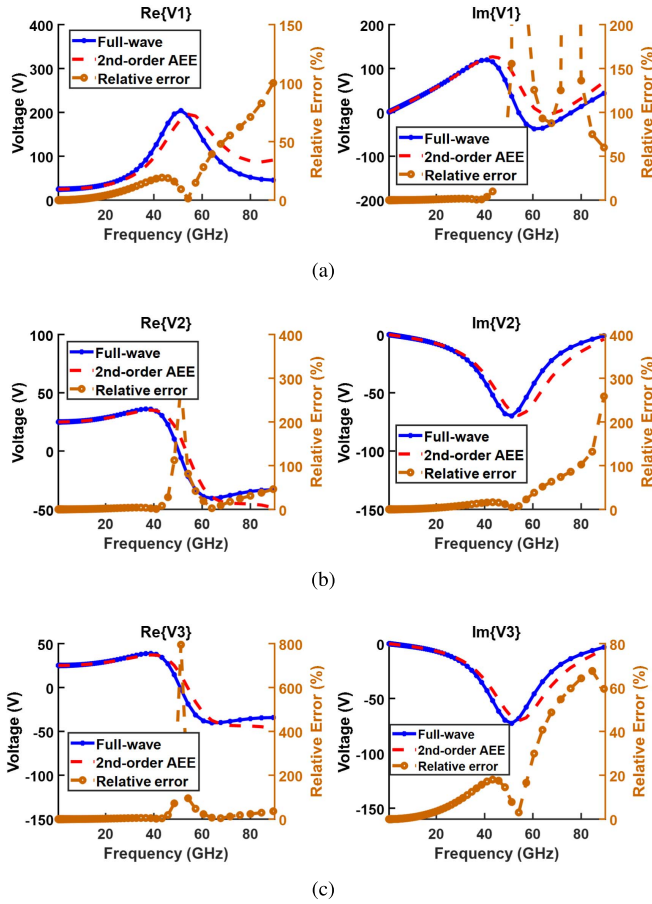
Fig. 11. Second-order AEE results by assuming constant eigenvectors versus full-wave analysis for example 2. (a) Voltage at port 1. (b) Voltage at port 2. (c) Voltage at port 3.
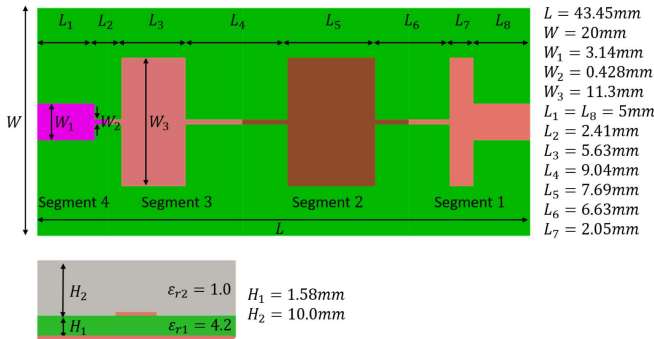

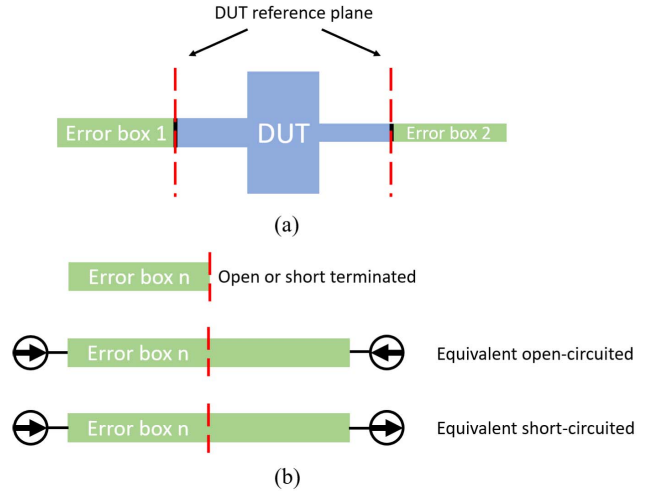Fig. 12. Geometry and dimensions of a low-pass filter.

Fig. 13. Illustration of deembedding procedure. (a) Cascade of the DUT and error boxes. (b) Mirrored models of the open- and short-circuited error box.
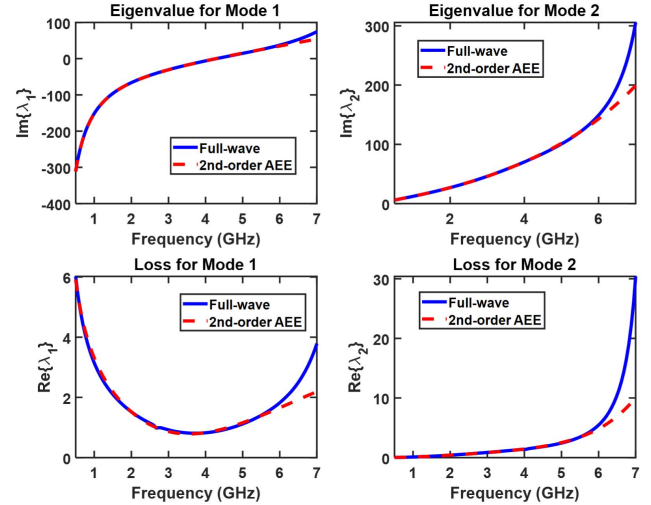

Fig. 14. Eigenvalues for segment 1 of the filter. Top: imaginary parts. Bottom: losses for each mode.

the entire device. To eliminate the effect of the excitation at the ports, the short-open calibration based deembedding technique [22], [23] is adopted. Otherwise, the cascading will give an incorrect result due to the distorted field distribution at the excitation ports. To illustrate the procedure of the deembedding technique, consider the diagram shown in Fig. 13 where the original geometry, also known as the device under test (DUT), is extended at both ports, and the extensions are termed as error boxes. A full-wave simulation is performed first to obtain the S-parameters of the extended structure.

By open- and short-circuiting the error boxes at the DUT reference planes, the ABCD matrices of the error boxes are computed from full-wave simulation. Through mathematical manipulation, the characteristics of the DUT can be calculated by eliminating the contributions of the error boxes from the global S-parameters. A detailed formulation can be found in [23]. Once the ABCD matrices are obtained for all the segments, the ABCD matrix for the entire device can be obtained by multiplying the ABCD matrices of the segments consecutively. Alternatively, the S-parameters of the whole device can be obtained directly from the S-parameters of the segments through cascading as illustrated in [24], which is more general but less straightforward.

The eigenvalues and eigenvectors for segment 1 are shown in Figs. 14 and 15. The four frequencies used for the AEE are selected equally between 0.5 and 5.5 GHz for the desired frequency range up to 5.5 GHz; however, the results are plotted
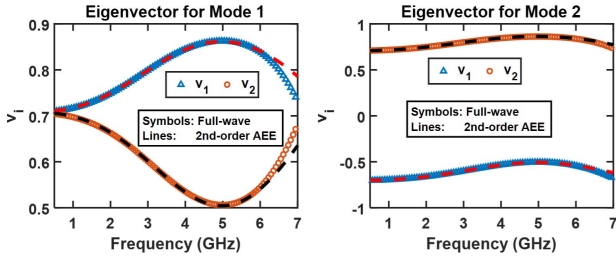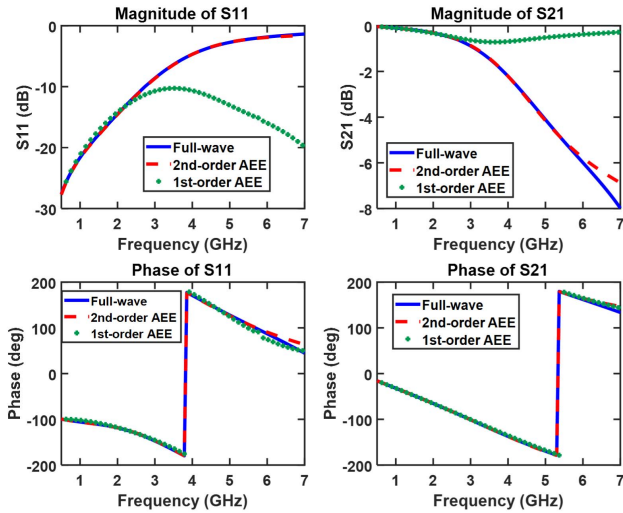
Fig. 15. Eigenvectors for segment 1 of the filter.

Fig. 16. *S*-parameters of segment 1 of the filter. Top: magnitude. Bottom: phase.

TABLE I
COMPUTATIONAL COSTS FOR THE SIMULATION OF THE LOW-PASS FILTER

Approaches	Time Cost (s)
Full-wave Direct	4318.40
Full-wave Cascading	6953.21
Second-order AEE Cascading	278.13

up to 7 GHz to show the behavior of the AEE beyond its intended range. For a two-port circuit, the submatrices in the "eigenvector-eigenvalue identity" are the input impedance at one port while leaving the other port open. It is interesting to observe that for all segments the eigenvalues of the submatrices start with a negative imaginary part and are capacitively dominant at low frequencies (C-type eigenvalues). As has been studied by the antenna community [25], the series resonance is a natural resonance that occurs in the input impedance of an antenna. The magnitude and phase of the *S*-parameters for segment 1 are given in Fig. 16, and to demonstrate the better performance of the second-order AEE, the results of the first-order AEE based on 0.5 and 2.2 GHz are also shown for comparison. As can be seen, the first-order AEE achieves a very good accuracy up to 2.5 GHz whereas the agreement of the second-order AEE reaches up to 6 GHz. The characteristics of other segments are obtained similarly and then cascaded together to obtain the characteristics of the entire device.
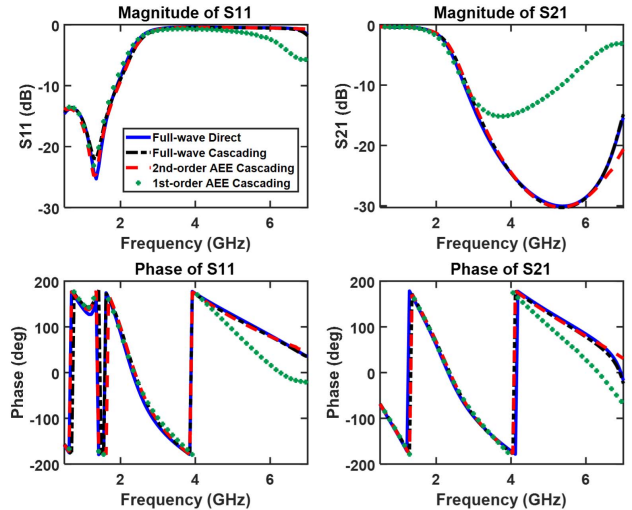

Fig. 17. *S*-parameters of the low-pass filter. Top: magnitude. Bottom: phase. Blue line: full-wave direct. Black line: full-wave cascading. Red line: second-order AEE cascading. Green plus sign: first-order AEE cascading.

Fig. 17 compares the AEE results and the full-wave solutions for the entire device. Note that the deembedding technique is applied not only to the four segments but also to the entire structure to remove the effects of all excitations and make the results comparable. The original geometries shown in Fig. 12 are considered to be the DUT and all excitation ports are fed by 9-mm extensions. Excellent agreement is achieved except for S_{11} at low frequencies. The curves of the AEE with cascading match very well with those of the full-wave solution. The discrepancy between the direct and cascaded analyses comes from the fact that only the quasi-TEM mode is considered and all higher-order modes are ignored in deembedding and cascading. The computational costs are listed in Table I to show the efficiency of the proposed approach. The full-wave analysis sweeps from 0.5 to 7 GHz with 106 points whereas the second-order AEE requires full-wave results at only four frequency points. The cascaded full-wave results have a larger cost than the direct analysis due to port extensions of each segment and the additional full-wave simulation of these extensions. Nevertheless, a speedup of 15.5 is still achieved for a fast evaluation of the filter with the use of the second-order AEE.

IV. CONCLUSION

A second-order AEE approach has been proposed and investigated to achieve a fast frequency sweep for efficient numerical modeling of passive RF circuits. In this approach, the *Z*-parameters are first extracted from a full-wave analysis, and the eigenvalue decomposition is then performed to obtain the eigenmodes. Second-order series or parallel *RLC* circuits are employed to model the eigenvalue for each mode. To capture the frequency dependence of the eigenvectors, an "eigenvector-eigenvalue identity" is adopted where the magnitude of each component in the eigenvectors can be constructed from the eigenvalues of the matrix as well as its submatrices. Only four frequency points are required to extract

all the characteristic parameters, and as a result, the frequency response of the device can be predicted over a broad frequency range. It has been found that the second-order AEE is very accurate for frequencies up to the point where the electrical size of the circuit reaches one wavelength. More *RLC* blocks can be added to increase the order of the approach and extend the validity to even higher frequencies, but the cost will also increase. If the circuit size is large, one can divide the entire structure into smaller segments and then cascade their characteristics together. The second-order AEE has been found to be very efficient and fast because one has to compute the characteristic modes at only four frequencies—instead of at many frequencies as in the direct full-wave analysis—to capture the variations in the frequency response.

REFERENCES

[1] A. E. Ruehli, "Equivalent circuit models for three-dimensional multi-conductor systems," *IEEE Trans. Microw. Theory Techn.*, vol. MTT-22, no. 3, pp. 216–221, Mar. 1974.

[2] R. Mittra, W. D. Becker, and P. H. Harms, "A general purpose Maxwell solver for the extraction of equivalent circuits of electronic package components for circuit simulation," *IEEE Trans. Circuits Syst. I, Fundam. Theory Appl.*, vol. 39, no. 11, pp. 964–973, Nov. 1992.

[3] T. Mangold and P. Russer, "Full-wave modeling and automatic equivalent-circuit generation of millimeter-wave planar and multilayer structures," *IEEE Trans. Microw. Theory Techn.*, vol. 47, no. 6, pp. 851–858, Jun. 1999.

[4] L. Zhu and K. Wu, "Unified equivalent-circuit model of planar discontinuities suitable for field theory-based CAD and optimization of M(H)MIC's," *IEEE Trans. Microw. Theory Techn.*, vol. 47, no. 9, pp. 1589–1602, Sep. 1999.

[5] L. Zhu and K. Wu, "Short-open calibration technique for field theory-based parameter extraction of lumped elements of planar integrated circuits," *IEEE Trans. Microw. Theory Techn.*, vol. 50, no. 8, pp. 1861–1869, Aug. 2002.

[6] H. Li, J. Jin, D. Jachowski, R. Silver, and R. Hammond, "Quasi-static numerical modeling of miniature RF circuits based on lumped equivalent circuits," *Int. J. Numer. Model., Electron. Netw., Devices Fields*, vol. 34, no. 1, p. e2795, Jan. 2021, doi: 10.1002/jnm.2795.

[7] G. J. Burke, E. K. Miller, S. Chakrabarti, and K. Demarest, "Using model-based parameter estimation to increase the efficiency of computing electromagnetic transfer functions," *IEEE Trans. Magn.*, vol. 25, no. 4, pp. 2807–2809, Jul. 1989.

[8] K. Kottapalli, T. K. Sarkar, R. Adve, Y. Hua, E. K. Miller, and G. J. Burke, "Accurate computation of wideband response of electromagnetic systems utilizing narrowband information," *Comput. Phys. Commun.*, vol. 68, nos. 1–3, pp. 126–144, Nov. 1991.

[9] L. T. Pillage and R. A. Rohrer, "Asymptotic waveform evaluation for timing analysis," *IEEE Trans. Comput.-Aided Design Integr. Circuits Syst.*, vol. 9, no. 4, pp. 352–366, Apr. 1990.

[10] M. A. Kolbehdari, M. Srinivasan, M. S. Nakhla, Q.-J. Zhang, and R. Achar, "Simultaneous time and frequency domain solutions of EM problems using finite element and CFH techniques," *IEEE Trans. Microw. Theory Techn.*, vol. 44, no. 9, pp. 1526–1534, Sep. 1996.

[11] M. Li, Q.-J. Zhang, and M. Nakhla, "Finite difference solution of EM fields by asymptotic waveform techniques," *IEE Proc.-Microw., Antennas Propag.*, vol. 143, no. 6, pp. 512–520, Dec. 1996.

[12] P. Feldmann and R. W. Freund, "Efficient linear circuit analysis by Padé approximation via the Lanczos process," *IEEE Trans. Comput.-Aided Design Integr. Circuits Syst.*, vol. 14, no. 5, pp. 639–649, May 1995.

[13] M. Celik and A. C. Cangellaris, "Simulation of dispersive multiconductor transmission lines by Padé approximation via the Lanczos process," *IEEE Trans. Microw. Theory Techn.*, vol. 44, no. 12, pp. 2525–2535, Dec. 1996.

[14] R. W. Freund, "Reduced-order modeling techniques based on Krylov subspaces and their use in circuit simulation," in *Applied and Computational Control, Signals, and Circuits*, vol. 1, B. N. Datta, Ed. Boston, MA, USA: Birkhäuser, 1999, pp. 435–498.

[15] Z. Bai and R. W. Freund, "A partial Padé-via-Lanczos method for reduced-order modeling," *Linear Algebra Appl.*, vols. 332–334, pp. 139–164, Aug. 2001.

[16] C. K. Aanandan, P. Debernardi, R. Orta, R. Tascone, and D. Trinchero, "Problem-matched basis functions for moment method analysis—An application to reflection gratings," *IEEE Trans. Antennas Propag.*, vol. 48, no. 1, pp. 35–40, Jan. 2000.

[17] F. Bertazzi, O. A. Peverini, M. Goano, G. Ghione, R. Orta, and R. Tascone, "A fast reduced-order model for the full-wave FEM analysis of lossy inhomogeneous anisotropic waveguides," *IEEE Trans. Microw. Theory Techn.*, vol. 50, no. 9, pp. 2108–2114, Sep. 2002.

[18] S.-H. Lee and J.-M. Jin, "Adaptive solution space projection for fast and robust wideband finite-element simulation of microwave components," *IEEE Microw. Wireless Compon. Lett.*, vol. 17, no. 7, pp. 474–476, Jul. 2007.

[19] H. Li, J.-M. Jin, D. R. Jachowski, and R. B. Hammond, "Fast frequency sweep analysis of passive miniature RF circuits based on analytic extension of eigenvalues," *IEEE Trans. Microw. Theory Techn.*, vol. 69, no. 1, pp. 4–14, Jan. 2021.

[20] P. B. Denton, S. J. Parke, T. Tao, and X. Zhang, "Eigenvectors from eigenvalues: A survey of a basic identity in linear algebra," 2019, *arXiv:1908.03795*. [Online]. Available: http://arxiv.org/abs/1908.03795

[21] D. M. Pozar, *Microwave Engineering*, 4th ed. Hoboken, NJ, USA: Wiley, 2012.

[22] L. Zhu and K. Wu, "Comparative investigation on numerical de-embedding techniques for equivalent circuit modeling of lumped and distributed microstrip circuits," *IEEE Microw. Wireless Compon. Lett.*, vol. 12, no. 2, pp. 51–53, Feb. 2002.

[23] V. I. Okhmatovski, J. Morsey, and A. C. Cangellaris, "On deembedding of port discontinuities in full-wave CAD models of multiport circuits," *IEEE Trans. Microw. Theory Techn.*, vol. 51, no. 12, pp. 2355–2365, Dec. 2003.

[24] K. Zhang, C.-F. Wang, and J.-M. Jin, "A hybrid FETD-GSM algorithm for broadband full-wave modeling of resonant waveguide devices," *IEEE Trans. Microw. Theory Techn.*, vol. 65, no. 9, pp. 3147–3158, Sep. 2017.

[25] K. A. Obeidat, B. D. Raines, and R. G. Rojas, "Discussion of series and parallel resonance phenomena in the input impedance of antennas," *Radio Sci.*, vol. 45, no. 6, pp. 1–9, Dec. 2010.
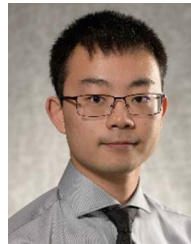
Hongliang Li (Graduate Student Member, IEEE) was born in Luohe, Henan, China, in 1994. He received the B.S. degree in electrical engineering and information science from the University of Science and Technology of China, Hefei, China, in 2017, and the M.S. degree in electrical and computer engineering from the University of Illinois at Urbana–Champaign, Urbana, IL, USA, in 2020, where he is currently pursuing the Ph.D. degree in electrical engineering.

Since 2017, he has been a Research Assistant with the Center for Computational Electromagnetics, University of Illinois at Urbana–Champaign. His research interests include the time- and frequency-domain finite-element methods, numerical modeling of electrical machines and RF circuits, and the development of fast algorithms.

Jian-Ming Jin (Fellow, IEEE) is currently the Y. T. Lo Chair Professor with the Department of Electrical and Computer Engineering and the Director with the Electromagnetics Laboratory and the Center for Computational Electromagnetics, University of Illinois at Urbana–Champaign, Urbana, IL, USA. He has authored or coauthored more than 280 articles in refereed journals and 22 book chapters. He has also authored *The Finite Element Method in Electromagnetics* (Wiley, First Edition, 1993, Second Edition, 2002, and Third Edition, 2014), *Electromagnetic Analysis and Design in Magnetic Resonance Imaging* (CRC, 1998), and *Theory and Computation of Electromagnetic Fields* (Wiley, First Edition 2010 and Second Edition 2015) and coauthored *Computation of Special Functions* (Wiley, 1996), *Fast and Efficient Algorithms in Computational Electromagnetics* (Artech, 2001), and *Finite Element Analysis of Antennas and Arrays* (Wiley, 2008). His current research interests include computational electromagnetics, multiphysics modeling, scattering and antenna analysis, electromagnetic compatibility, high-frequency circuit modeling and analysis, bioelectromagnetics, and magnetic resonance imaging.

Dr. Jin was elected by the ISI as one of the world's most cited authors in 2002 and is also a Fellow of the Optical Society of America, the Electromagnetics Academy, and the Applied Computational Electromagnetics Society (ACES). He was a recipient of the 1994 National Science Foundation Young Investigator Award, the 1995 Office of Naval Research Young Investigator Award, the 1999 ACES Valued Service Award, the 2014 ACES Technical Achievement Award, the 2015 IEEE APS Chen-To Tai Distinguished Educator Award, the 2015 and 2020 IEEE Edward E. Altschuler AP-S Magazine Prize Paper Awards, the 2016 ACES Computational Electromagnetics Award, the 2017 IEEE APS Harrington-Mittra Computational Electromagnetics Award, and the 2020 ECE Distinguished Educator Award from the University of Michigan. He was awarded Adjunct, Visiting, Guest, or Chair Professorship by 14 institutions around the world and appointed an IEEE AP-S Distinguished Lecturer in 2015. He was also a recipient of the 1997 and 2000 Xerox Research Awards and was appointed as the First Henry Magnuski Outstanding Young Scholar in 1998 and later as a Sony Scholar in 2005 at the University of Illinois at Urbana–Champaign. His name appeared 24 times in the University's List of Excellent Instructors. His students have received the best paper awards in the IEEE 16th Topical Meeting on Electrical Performance of Electronic Packaging and 25th, 27th, 31st, and 32nd Annual Review of Progress in Applied Computational Electromagnetics. He was an Associate Editor and Guest Editor of the IEEE TRANSACTIONS ON ANTENNAS AND PROPAGATION, *Radio Science, Electromagnetics, Microwave and Optical Technology Letters*, and *Medical Physics*, and now serves as an Editor-in-Chief for the *International Journal of Numerical Modeling: Electronic Networks, Devices and Fields*.

Douglas R. Jachowski (Member, IEEE) received the B.S. and M.S. degrees in electrical engineering from Stanford University, Stanford, CA, USA, in 1981 and 1987, respectively.

From 1982 to 1987, he designed circuits, instruments, and integrated sensors at MEMS pioneers Transensory Devices and NovaSensor, both of Fremont, CA. While moonlighting in 1984, he co-developed the first self-tuning transmitter combiner. From 1988 to 1994, as the Director of Filter Technology for Allen Telecom, Reno, NV, USA, he designed microwave filters for cell phone base stations and pioneered the use of dielectric resonators in commercial applications. Following a period as a consultant, he joined the Naval Research Laboratory (NRL), Washington, DC, USA, in 2003, where his research focused on absorptive and tunable filters and reconfigurable receiver front ends. He was the Head of the Solid-State Circuits Section, NRL, from 2009 to 2012, before returning to consulting. In 2016, he joined Resonant Inc., Goleta, CA, where he designs SAW and BAW multiplexers and works to improve acoustic-wave filter technology and design techniques.

Robert B. Hammond (Life Member, IEEE) received the B.S., M.S., and Ph.D. degrees in physics and applied physics from Caltech, Pasadena, CA, USA, in 1971, 1972, and 1976, respectively.

Under thesis advisors J. W. Mayer and T. C. McGill, he measured for the first time the thermodynamic properties of the electron–hole-liquid in silicon and the splitting of the silicon exciton ground state. From 1976 to 1987, he was with the Los Alamos National Laboratory, Los Alamos, NM, USA, where he led Electronics Research and Exploratory Development, and established a semiconductor physics and device development group. He led the development of a variety of novel materials, devices, and instruments, including subnanosecond radiation detectors and multigigawatt switches, subpicosecond electrical characterization measurements, and laser position sensors and beam diagnostics. He contributed to the understanding of the fundamental mechanisms of pulsed laser annealing in silicon and the fundamental properties of highly excited silicon at low temperature. In 1987, he co-founded Superconductor Technologies Inc. (STI), Santa Barbara, CA, where he was the Chief Technical Officer through 2012. At STI, he built a team of engineers and scientists, lead technology development, and directed corporate technology strategy, and intellectual property. He participated in raising >\$250M in investment capital, led the company for the two years preceding its successful IPO in 1993, and attracted and successfully executed against >\$100M in DARPA technology development funding. Under his leadership, STI pioneered the development and manufacturing of superconducting TlBaCaCuO and YBaCuO thin films, superconducting wireless microwave filter chips, and a no-maintenance Stirling cryocooler, all incorporated in STI's flagship product SuperLink. These RF front-end systems ultimately operated 24/7 in 7000 cellular base stations across USA. In 2012, he co-founded Resonant Inc., Goleta, CA, where he is currently the Chief Technical Officer. Resonant Inc., designs SAW and BAW filters and multiplexers for RF front-end applications in smartphones. Resonant Inc., recently invented a new acoustic filter technology, XBAR, that promises to address the many novel emerging requirements for RFFE filtering in 5G smartphones. He has authored 100 technical papers and holds several dozen patents.